Marquette University
e-Publications@Marquette

Physics Faculty Research and Publications   Physics, Department of

10-19-2007

Evidence for a Dinuclear Active Site in the Metallo-β-lactamase BcII with Substoichiometric Co(II): A New Model for Uptake

Leticia l. Llarrull
University of Notre Dame

Mariana F. Tioni
Universidad Nacional de Rosario

Jason M. Kowalski
Medical College of Wisconsin

Brian Bennett
Marquette University, brian.bennett@marquette.edu

Alejandro J. Vila
Universidad Nacional de Rosario

Evidence for a Dinuclear Active Site in the Metallo-β-lactamase BcII with Substoichiometric Co(II)
A NEW MODEL FOR METAL UPTAKE*[S]

Leticia I. Llarrull[‡1,2], **Mariana F. Tioni**[‡1,3,4], **Jason Kowalski**[§], **Brian Bennett**[§5], **and Alejandro J. Vila**[‡4,6]

From the [‡]Molecular Biology Division, Instituto de Biología Molecular y Celular de Rosario, Consejo Nacional de Investigaciones Científicas y Técnicas de Argentina, and Biophysics Section, Facultad de Ciencias Bioquímicas y Farmacéuticas, Universidad Nacional de Rosario, Suipacha 531, S2002LRK Rosario, Argentina and the [§]National Biomedical EPR Center, Department of Biophysics, Medical College of Wisconsin, Milwaukee, Wisconsin 53226-0509

Metallo-β-lactamases are zinc-dependent enzymes that constitute one of the main resistance mechanisms to β-lactam antibiotics. Metallo-β-lactamases have been characterized both in mono- and dimetallic forms. Despite many studies, the role of each metal binding site in substrate binding and catalysis is still unclear. This is mostly due to the difficulties in assessing the metal content and site occupancy in solution. For this reason, Co(II) has been utilized as a useful probe of the active site structure. We have employed UV-visible, EPR, and NMR spectroscopy to study Co(II) binding to the metallo-β-lactamase BcII from *Bacillus cereus*. The spectroscopic features were attributed to the two canonical metal binding sites, the 3H (His[116], His[118], and His[196]) and DCH (Asp[120], Cys[221], and His[263]) sites. These data clearly reveal the coexistence of mononuclear and dinuclear Co(II)-loaded forms at Co(II)/enzyme ratios as low as 0.6. This picture is consistent with the macroscopic dissociation constants here determined from competition binding experiments. A spectral feature previously assigned to the DCH site in the dinuclear species corresponds to a third, weakly bound Co(II) site. The present work emphasizes the importance of using different spectroscopic techniques to follow the metal content and localization during metallo-β-lactamase turnover.

MβLs[7] belong to a group of hydrolytic enzymes that constitute one of the main resistance mechanisms to β-lactam antibiotics that has evolved in bacteria since the introduction of these compounds in clinical treatments (1–5). The ability of MβLs to hydrolyze the amide bond of the β-lactam ring characteristic of this group of antibiotics depends on the presence of one or two Zn(II) ions bound to their active sites (2, 5). MβLs display an unusually broad substrate profile and are not susceptible to clinically used inhibitors of the well known serine-β-lactamases. Increasingly frequent reports of transmission of MβL genes among pathogenic and opportunistic bacteria indicate that bacteria expressing these enzymes pose a significant threat to public health (3).

The design of therapeutically useful inhibitors for these enzymes has been unsuccessful so far. The diverse substrate preferences of MβLs may preclude the discovery or design of a universal inhibitor with both efficacy and specificity toward all MβLs. Despite extensive study, there is still great controversy regarding the metal content in the catalytically relevant species and on the mechanisms of action of MβLs (2, 6–13). The elusive nature of intermediates and transition states during the reaction has hampered rational inhibitor design. This scenario prompts for a detailed characterization of the different active species and their metal content in the resting state form and during turnover.

BcII, the MβL from *Bacillus cereus*, has been extensively characterized, thus representing a prototypical enzyme for mechanistic studies. BcII was first crystallized with only one Zn(II) ion tetrahedrally coordinated to three His residues (His[116], His[118], and His[196]) and an H_2O/OH^- molecule (14), in the so-called 3H site (14) (Fig. 1A). Spectroscopic experiments (10) and a second crystal structure later indicated that BcII was also capable of binding a second metal ion (15, 16), which is trigonal bipyramidally coordinated to Asp[120], Cys[221], His[263], a H_2O/OH^- bridging the two metal ions, and an additional water molecule. This site is known as the DCH site (Fig. 1B). Further spectroscopic studies revealed that when the apoenzyme is reconstituted with 1 eq of Zn(II), Cd(II), or Co(II), the metal ion is distributed between both binding sites, instead of following an ordered, sequential binding (8, 10, 17, 18). In addition, some of these data suggested that formation of the dinuclear species takes place only at a metal/BcII ratio larger than 1 (8). Knowing
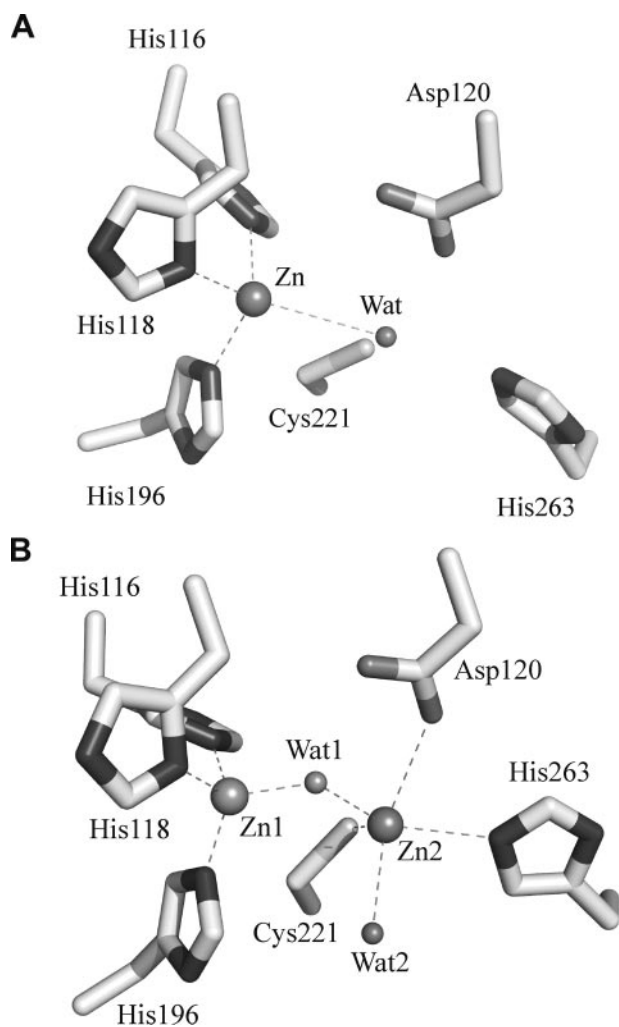
FIGURE 1. **Active sites of mono-Zn(II) BcII (A) and di-Zn(II) BcII (B).** The images were rendered with PyMol (DeLano Scientific LLC) from Protein Data Bank files 1bmc and 1bc2, respectively. Zinc atoms are rendered as *large spheres*, and solvent molecules are rendered as *small spheres*.

the identity of the metallated species formed at increasing metal concentration is specially important if we recall recent studies that suggest that Co(II)-BcII is only active in its dinuclear form (19).

Metal binding studies on the homologous MβL CcrA from *Bacteroides fragilis* have shown a different metal binding mechanism (20). Co(II) uptake by apo-CcrA was strictly sequential, as shown by several spectroscopic techniques. At a Co(II)/CcrA ratio equal to 1, only the 3H site becomes occupied, whereas the DCH site is metallated upon the addition of a second Co(II) equivalent. No evidence of redistribution ("scrambling") of the metal ion between the two binding sites was found for this enzyme (20).

Co(II) can be exploited as a unique spectroscopic probe of the catalytic mechanism of MβLs by following its spectral features during turnover (7, 21, 22). We decided to characterize in detail the identity and metal content of the Co(II)-BcII adducts formed at different Co(II)/BcII ratios prior to any mechanistic study. By using UV-visible, EPR, and NMR spectroscopy, as well as through measurements of the Co(II) binding constants, we have determined that 1) BcII is able to bind up to 3 Co(II) eq in its active site and that some of the features previously

assigned to the DCH site in the dinuclear species correspond to a third, weakly bound Co(II) site, 2) a di-Co(II) species is formed at a Co(II)/BcII ratio as low as 0.6, and 3) different species coexist in equilibrium at very low (<1) Co(II)/BcII ratios. These observations prompt for a reinterpretation of previous studies on Co(II)-substituted BcII and suggest that the catalytic mechanism of this enzyme cannot be analyzed without considering the different coexisting species.

EXPERIMENTAL PROCEDURES

Reagents—All chemicals were of the highest quality available. The MTPBS buffer was 16 mM Na_2HPO_4, 4 mM NaH_2PO_4, and 150 mM NaCl, pH 7.3. *Escherichia coli* BL21(DE3)pLysS′ cells (Stratagene) were employed for protein production. Luria-Bertani (LB) medium (Sigma) was used as growth medium for all bacterial strains.

DNA Techniques and Cloning Procedure—DNA preparation and related techniques were performed according to standard protocols (23). Plasmid DNA was isolated using the Wizard Plus SV Minipreps kit (Promega).

Enzyme Purification—Wild type BcII was expressed in *E. coli* BL21(DE3)pLysS′ as a fusion protein with glutathione *S*-transferase (10), purified, and quantified as follows. Typically, the cell pellet obtained from 50 ml of a culture in late logarithmic phase in LB medium supplemented with 150 μg/ml ampicillin and 35 μg/ml chloramphenicol was resuspended in fresh medium and used to inoculate 1 liter of LB medium supplemented with 150 μg/ml ampicillin and 35 μg/ml chloramphenicol in a 5-liter Erlenmeyer flask. Cells were grown for 2 h at 37 °C until $A_{600} = 1$ was reached. The expression of fusion protein was induced by the addition of 10 g of lactose, and the culture was further incubated at 37 °C for an additional 4-h period. All subsequent purification steps were performed at 4 °C. *E. coli* cells were disrupted by sonication in lysis buffer (MTPBS with 3.3 μg/ml DNase, 5 mM $MgCl_2$, and 1 mM phenylmethylsulfonyl fluoride), and cell debris was separated by ultracentrifugation. The GST-BcII fusion protein was purified by affinity chromatography using a glutathione-Sepharose resin (Amersham Biosciences), as previously reported (10). The pure fractions were treated with bovine plasma thrombin (Sigma) at a 1:100 ratio, after the addition of 150 mM NaCl, 2.5 mM $CaCl_2$, at 26 °C for 2 h. BcII was purified from the proteolysis mixture by ion exchange chromatography on Sephadex CM-50 (Amersham Biosciences) as previously reported (10). Protein samples were dialyzed against >100 volumes of 10 mM HEPES, pH 7.5, 0.2 M NaCl. Purity of the enzyme preparations was checked by SDS-PAGE. Protein concentration was measured spectrophotometrically using $\epsilon_{280} = 30,500$ M^{-1} cm^{-1} (18). Metal content in protein samples was checked using the colorimetric reagent 4-(2-pyridilazo)-resorcinol and ranged between 1.4 and 1.8 metal/total protein, depending on the enzyme preparation (24, 25).

Preparation of Apo-BcII—All buffer solutions used to prepare the apoenzyme were treated by extensive stirring with Chelex 100 (Sigma). Apo-BcII was prepared by dialysis of the purified holoprotein (~200 μM) against two changes of >100 volumes of 10 mM HEPES, pH 7.5, 0.2 M NaCl, 20 mM EDTA over a 12-h period. EDTA was removed from the resulting
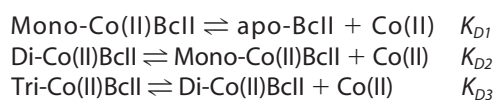
apoenzyme solution by three dialysis steps against >100 volumes of 10 mM HEPES, pH 7.5, 1 M NaCl, 0.3 g/liter Chelex 100; one dialysis step against >100 volumes of 10 mM HEPES, pH 7.5, 0.2 M NaCl, 0.3 g/liter Chelex 100; and finally two dialysis steps against >100 volumes of 100 mM HEPES, pH 7.5, 0.2 M NaCl, 0.3 g/liter Chelex 100. All dialysis steps were carried out at 4 °C, under stirring and for at least 6 h. Metal content in apoprotein samples was checked using the colorimetric reagent 4-(2-pyridilazo)-resorcinol (24, 25).

Electronic Spectroscopy of Co(II)-BcII Derivatives—A solution of 200–300 μM apo-BcII in 100 mM HEPES, pH 7.5, 0.2 M NaCl was titrated with a 10.6 mM CoSO$_4$ stock solution prepared in 100 mM HEPES, pH 7.5, 0.2 M NaCl. Spectra were recorded at room temperature in a Jasco 550 UV-visible spectrophotometer. The spectra were corrected for dilution upon adding Co(II), and the UV-visible difference spectra were obtained by subtracting the spectrum of apo-BcII.

The complete formation of the di-Co(II) adduct, as monitored by UV-visible spectroscopy, was achieved at a ratio of 1.4–1.8 Co(II)/total protein, depending on the enzyme preparation. In all preparations, the level of Co(II) uptake of the apoenzymes paralleled the original Zn(II) content of the protein as isolated. The concentration of "metallable" protein was then calculated by multiplying the concentration of protein determined by absorbance at 280 nm by the factor $n/2$, where n is the number of analytical Co(II) equivalents needed to reach the maximum intensity of the d-d (550 nm) and CT (343 nm) bands. At this Co(II) concentration, all of the metallable protein is in the dinuclear form. The protein concentration used in the different fits was then calculated by employing this correction factor, to account for the variable fraction of protein capable of binding metal.

The changes in absorbance at 343, 383, and 550 nm with increasing Co(II) concentrations were fit simultaneously using the program DynaFit (BioKin, Ltd.) (26). The data were fit to the following model (Model 1).

$$\text{Mono-Co(II)BcII} \rightleftharpoons \text{apo-BcII} + \text{Co(II)} \qquad K_{D1}$$
$$\text{Di-Co(II)BcII} \rightleftharpoons \text{Mono-Co(II)BcII} + \text{Co(II)} \qquad K_{D2}$$
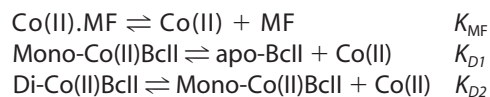$$\text{Tri-Co(II)BcII} \rightleftharpoons \text{Di-Co(II)BcII} + \text{Co(II)} \qquad K_{D3}$$
MODEL 1

The model assumes that the mono-Co(II) species is a mixture of two enzyme species, one with cobalt bound to the 3H site (which absorbs at 550 nm) and a second species with metal bound to the DCH site (which absorbs at 343 nm). Di-Co(II) BcII presents both metal binding sites loaded and absorbs at 550 and 343 nm, and the tri-Co(II) species absorbs at 550 nm and at 383 nm.
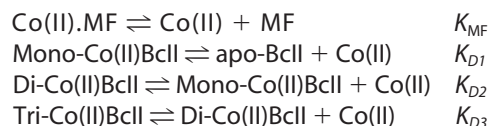
Metal Binding Affinities Measured with Mag-fura-2—The dissociation constants were estimated from competition experiments with the chromophoric chelator Mag-fura-2 (MF; Molecular Probes, Eugene, OR) (8). The indicator was first titrated with Co(II) at 30 °C, and changes in absorbance at 363 nm with added metal were fit with DynaFit to obtain the dissociation constant of Co(II) from the complex with Mag-fura-2 (K_{MF}) in 100 mM HEPES, pH 7.5, 0.2 M NaCl. A value of 2.8 ± 0.1 μM was obtained, with $\epsilon_{MF,\ 363\ nm} = 22,000 \pm 100\ \text{M}^{-1}\ \text{cm}^{-1}$ and $\epsilon_{Co(II)\cdot MF,\ 363\ nm} = 4,510 \pm 140\ \text{M}^{-1}\ \text{cm}^{-1}$. Afterward, a solution of 2.7 μM Mag-fura-2 in 100 mM HEPES, pH 7.5, 0.2 M

NaCl was titrated with Co(II) in the presence of 1–3 μM apo-BcII, using a 1.12 mM CoSO$_4$ stock solution in the same buffer, at 30 °C. The changes in absorbance at 363 nm with added metal, obtained from experiments carried out with three different apoprotein concentrations, were fit together to two different models, using the program DynaFit, in order to calculate K_{D1} and K_{D2}. The first model (Model 2, described below) involves three dissociation equilibria, where K_{MF} was fixed to the value determined independently.

$$\text{Co(II).MF} \rightleftharpoons \text{Co(II)} + \text{MF} \qquad K_{MF}$$
$$\text{Mono-Co(II)BcII} \rightleftharpoons \text{apo-BcII} + \text{Co(II)} \qquad K_{D1}$$
$$\text{Di-Co(II)BcII} \rightleftharpoons \text{Mono-Co(II)BcII} + \text{Co(II)} \qquad K_{D2}$$
MODEL 2

A second model involving four dissociation equilibria (Model 3, presented below), was also considered. K_{MF} and K_{D3} were fixed to the values determined independently, from Co(II) binding to MF and from the UV-visible titration of apo-BcII with Co(II), respectively.

$$\text{Co(II).MF} \rightleftharpoons \text{Co(II)} + \text{MF} \qquad K_{MF}$$
$$\text{Mono-Co(II)BcII} \rightleftharpoons \text{apo-BcII} + \text{Co(II)} \qquad K_{D1}$$
$$\text{Di-Co(II)BcII} \rightleftharpoons \text{Mono-Co(II)BcII} + \text{Co(II)} \qquad K_{D2}$$
$$\text{Tri-Co(II)BcII} \rightleftharpoons \text{Di-Co(II)BcII} + \text{Co(II)} \qquad K_{D3}$$
MODEL 3

EPR Spectroscopy—EPR spectroscopy was performed at either 13 K, 2 milliwatts, and 9.63 GHz ($\mathbf{B}_{\text{microwave}} \perp \mathbf{B}_{\text{static}}$) or 10 K, 50 milliwatts, and 9.37 GHz ($\mathbf{B}_{\text{microwave}} \parallel \mathbf{B}_{\text{static}}$), using a Bruker Elexsys E500 spectrometer equipped with an ER 4116 DM TE$_{012}$/TE$_{102}$ dual mode X-band cavity and an Oxford Instruments ESR-900 helium flow cryostat. EPR spectra were simulated with the matrix diagonalization program XSophe (Bruker Biospin) using a spin Hamiltonian $H = \beta g \cdot H \cdot S + S \cdot D \cdot S + S \cdot A \cdot I$ Least-squares fitting of simulations and experimental spectra was carried out using IGORPro (Wavemetrics). Recording conditions of 13 K and 2 milliwatts were determined to be nonsaturating for 0.5, 1.0, and 2.0 eq of Co(II) in frozen solutions of BcII. Integration of spectra thus recorded gave pseudoabsorption curves that lay on a level base line, providing further strong evidence that there were no selectively saturated species in the spectra of BcII with 1 and 2 eq of Co(II). Spectra recorded at up to 160 milliwatts and down to 3.6 K provided no evidence at all for any species with very fast relaxation, and the spectra under these conditions were typical for spectra of $M_S = \frac{1}{2}$ Co(II) under rapid passage conditions.

The apoprotein samples (~1 mM), in 100 mM HEPES, pH 7.5, 0.2 M NaCl, were titrated stepwise with a 6 mM CoSO$_4$ stock solution prepared in the same buffer. The Co(II)-containing solution was rapidly mixed with the sample in the EPR tube by manual flicking (27) and frozen in liquid nitrogen. For successive additions of Co(II), EPR samples were quickly thawed (~5 s) from 77 K to 20 °C by agitating the sample tube in water.

NMR Spectroscopy—NMR spectra were recorded on a Bruker Avance II 600 spectrometer operating at 600.13 MHz at different temperatures, as indicated. ^{1}H NMR spectra were recorded under conditions set to optimize detection of the fast
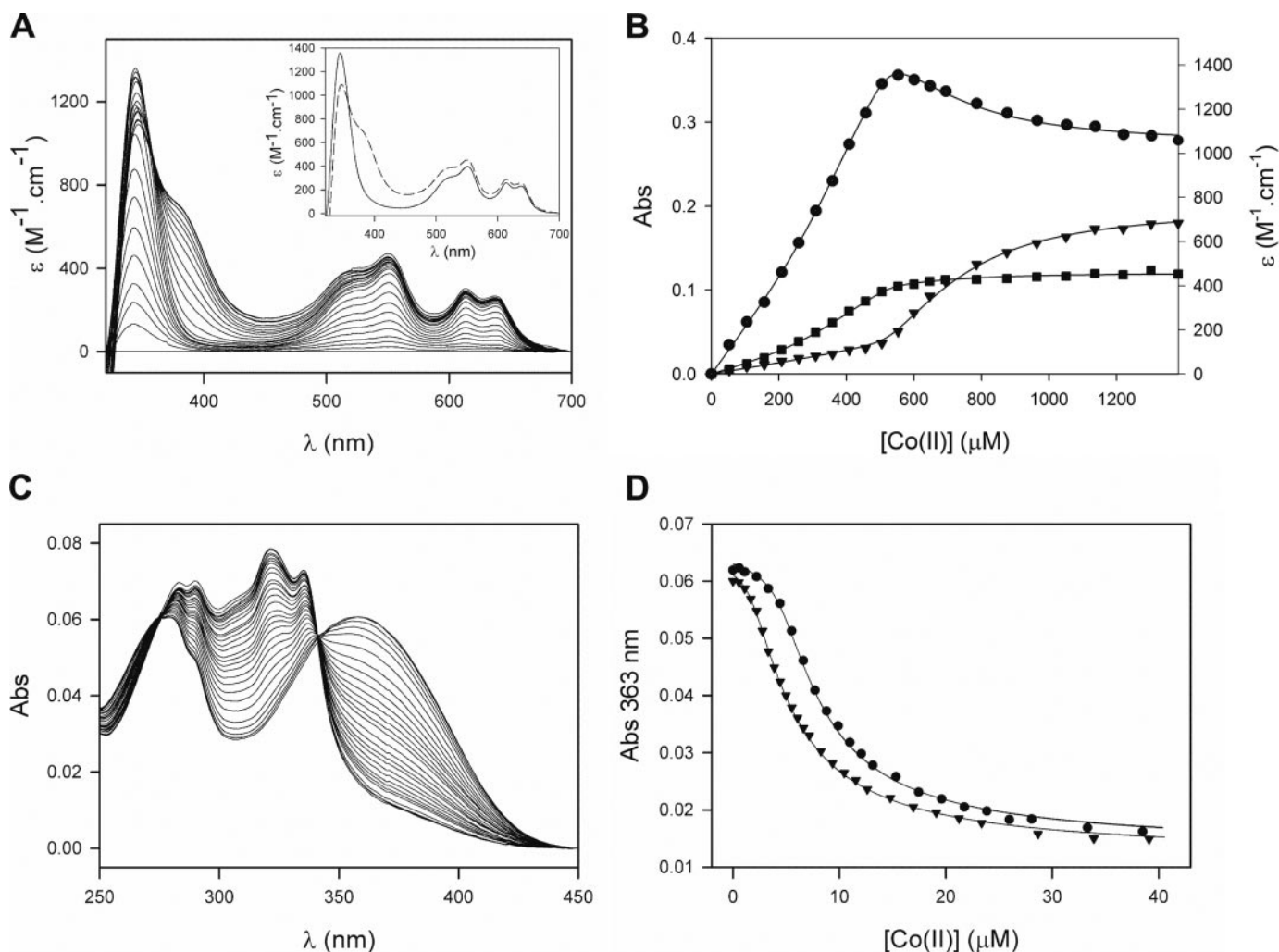
FIGURE 2. **Determination of the affinity of apo-BcII for Co(II).** *A*, UV-visible titration of 351 μM apo-BcII with 10.6 mM CoSO4 in 100 mM HEPES, pH 7.5, 0.2 M NaCl. Molar absorption values were calculated considering the concentration of protein capable of binding metal (263 μM), as described under "Experimental Procedures." The *inset* shows the spectra of di-Co(II) BcII (achieved in this experiment upon the addition of 1.5 Co(II) eq; *solid line*) and of BcII with excess Co(II) (4.0 Co(II) eq; *dashed line*). *B*, plot of the absorbance at 343 nm (*circles*), 383 nm (*inverted triangles*), and 550 nm (*squares*) as a function of the concentration of added Co(II) in the UV-visible titration. The *solid lines* correspond to the fit using Model 1 (see "Experimental Procedures"). *C*, titration of a solution containing 0.89 μM apo-BcII and 2.66 μM Mag-fura-2 with Co(II) in 100 mM HEPES, pH 7.5, 0.2 M NaCl, 30 °C. *D*, plot of the absorbance at 363 nm as a function of the concentration of added Co(II) for different competition experiments; the Mag-fura-2 concentration was ~2.7 μM in both experiments, and the apoprotein concentration was 0.89 μM (*inverted triangles*) and 2.21 μM (*circles*). The *solid line* corresponds to the fit using Model 2. The parameters obtained were $K_{D1} = 0.12 \pm 0.06$ μM, $K_{D2} = 0.16 \pm 0.04$ μM, $\epsilon_{MF, 363\,nm} = 22,000 \pm 100$ M^{-1} cm^{-1}, and $\epsilon_{Co(II)\cdot MF, 363\,nm} = 4,510 \pm 140$ M^{-1} cm^{-1}. The fit obtained with Model 3 (*dashed line*) superimposes with the curve obtained with Model 2. The parameters obtained with Model 3 were $K_{D1} = 0.10 \pm 0.06$ μM, $K_{D2} = 0.17 \pm 0.04$ μM, $\epsilon_{MF, 363\,nm} = 22,000 \pm 100$ M^{-1} cm^{-1}, and $\epsilon_{Co(II)\cdot MF, 363\,nm} = 4,510 \pm 140$ M^{-1}·cm^{-1}, with K_{D3} fixed in 94 μM.

relaxing paramagnetic resonances, using either the super-WEFT pulse sequence (28) or water presaturation. Spectra were acquired over large spectral widths with acquisition times ranging from 16 to 80 ms and intermediate delays from 2 to 35 ms. One-dimensional experiments with solvent presaturation were used to record isotropically shifted signals closer to the diamagnetic envelope. T_1 measurements were performed using the nonselective inversion-recovery method. One-dimensional NOE difference and NOESY spectra were obtained as described previously (29, 30), with mixing times of 5 and 25 ms.

The apoprotein samples (~1 mM), in 100 mM HEPES, pH 7.5, 0.2 M NaCl, were titrated stepwise with a 37.8 mM CoSO$_4$ stock solution prepared in the same buffer. Co(II) was added to the sample in the NMR tube. In order to obtain the spectra of the protein with excess Co(II) in D$_2$O, the sample with 3.5 eq of added cobalt was diafiltrated with 100 mM HEPES, pH 7.1 (pD

7.5), 0.2 M NaCl, containing the same concentration of Co(II) as the protein sample, in Amicon-Ultra-4 units (Millipore). A second titration was carried out in D$_2$O, with the apoprotein sample in 100 mM HEPES, pH 7.1 (pD 7.5), 0.2 M NaCl, by the stepwise addition of Co(II) from a 37.8 mM stock solution prepared in the same buffer.

No evidence of protein denaturation or aggregation was detected in any of the titration experiments (UV-visible, EPR, and NMR), even when working at high protein concentrations.

RESULTS

Spectrophotometric Titrations—The spectrum of Co(II)-substituted BcII with excess Co(II) is reported in the *inset* in Fig. 2*A* (*dashed line*); it presents two charge transfer bands at 343 and 383 nm (8) and a pattern of ligand field bands (530–640 nm) similar to the one reported for the alkaline form of Co(II)-car-

bonic anhydrase (31). These spectral features have been previously assigned to each of the metal binding sites in BcII. Davies and Abraham (32) early attributed the 343 nm absorption band to a ligand to metal charge transfer band due to the interaction of Co(II) with the Cys ligand in the DCH site. Later, a hybrid adduct was obtained, in which Zn(II) occupies the 3H site and Co(II) is located in the DCH site (10). This experiment demonstrated that the absorption features in the visible range are largely due to the 3H site, whereas the 343 nm band corresponds to the DCH site. A study performed under different conditions reported a new CT band at 383 nm (8). The authors attributed this band to the diCo(II)-BcII adduct while assigning the 343 nm band to a mononuclear form of the enzyme.

Titration of apo-BcII with Co(II) was followed by absorption spectroscopy in the UV-visible range (Fig. 2, *A* and *B*). The simultaneous buildup of the charge transfer band at 343 nm and of the d-d bands at <1 eq of Co(II) added confirms that, under these experimental conditions, the two metal sites are being filled at the same time, as already reported (8, 10) (Fig. 2, *A* and *B*). Saturation of both bands took place at a Co(II)/BcII ratio higher than 1 (ranging between 1.4 and 1.8, depending on the enzyme preparation), in contrast to the data reported by de Seny *et al.* (8), where saturation occurs at 1 Co(II) eq per BcII.

At concentrations of added Co(II) beyond this saturation point, three interesting features are observable in the data presented in Fig. 2*B*. The intensity of the band at 343 nm decreases asymptotically, and this is mirrored in an asymptotic increase in the intensity of the band at 383 nm, although neither of the intensities of the 343 and 383 nm bands plateaued completely, even at 4 eq of added Co(II). The third feature of note is that there is no significant change in the intensity of the d-d region of the spectrum. These spectral changes can be accounted for by the binding of Co(II) to BcII in a site that (i) exhibits higher than 4-fold coordination (with poorly resolved low intensity d-d bands) and (ii) perturbs the Co(II) ion already bound to the Cys ligand.

The fact that the d-d bands in the visible range (attributable to the 3H site) do not increase significantly with further Co(II) added after saturation of the 343 nm CT band clearly indicates that both metal sites are fully loaded at this point. Therefore, the spectrum obtained at this point corresponds to the di-Co(II) enzyme (Fig. 2*A*), as originally suggested by us (10). We used the point of saturation to calculate the effective metallable enzyme concentration, as described under "Experimental Procedures." From now on, the Co(II) eq refer to the corrected protein concentration. The CT band at 383 nm, which appears at higher Co(II)/BcII ratios would correspond to a third metal ion that perturbs the 343 nm signal (DCH site) without affecting the spectral features of the 3H site. The intensity of the 383 nm CT band was variable among different protein preparations, showing no correlation with the level of metal uptake to the dinuclear binding site.

The absorbance changes upon Co(II) uptake at 343, 383, and 550 nm could be fit to a model assuming binding of 2 Co(II) eq at a submicromolar range and a third one with lower affinity (see Model 1). The model assumes that the mono-Co(II) species is a mixture of two enzyme species, one with Co(II) bound to the 3H site (which hence absorbs only at 550 nm) and a second

species with metal bound to the DCH site (which absorbs at 343 nm). Di-Co(II) BcII presents both metal binding sites loaded and therefore absorbs at the same wavelengths, and a tri-Co(II) species is invoked that absorbs at 550 and 383 nm. From this experiment, we estimated the following macroscopic dissociation constants: $K_{D1} < 60$ nM, $K_{D2} = 0.6 \pm 0.2$ μM, $K_{D3} = 94 \pm 12$ μM. This experiment, as a previous related study (8), was performed at stoichiometric conditions for the first two binding sites and therefore cannot be used to retrieve accurate values for K_{D1} and K_{D2}. Nevertheless, it reveals the existence of a spectrophotometrically detectable event with a dependence on Co(II) that can be described by an apparent equilibrium constant of around 90 μM.

Cobalt(II) Binding to BcII by Competition Experiments—We studied Co(II) binding to apo-BcII by competition experiments with the chromophoric metal ligand Mag-fura-2, whose spectroscopic features change upon Co(II) binding. This procedure has already been employed to monitor Zn(II) and Cd(II) binding to apo-BcII (8). The spectra show an isosbestic point at 343 nm and maxima at 363 and 323 nm for the metal-free compound and the 1:1 Co(II) complex, respectively (Fig. 2*C*). The titration data could be accounted for by considering a model with two binding equilibria (Model 2), resulting in submicromolar dissociation constants ($K_{D1} = 0.12 \pm 0.06$ μM and $K_{D2} = 0.16 \pm 0.04$ μM; Fig. 2*D*). The competition experiments of apo-BcII with Mag-fura-2 could also be fit to a model involving three equilibria (Model 3) (*i.e.* taking into account the third metal ion bound to BcII). However, since the constant for the third equilibrium (K_{D3}), as estimated from the UV-visible titration, is almost 34 times larger than the dissociation constant of Co(II) to Mag-fura-2, this third binding site is incapable of competing with Mag-fura-2 for Co(II), and K_{D3} cannot be estimated from these competition experiments. Consequently, we decided to fit the competition data with the three-equilibrium model but fixing the K_{D3} value to the one determined from the UV-visible titration. With this assumption, it is possible to obtain values for the macroscopic dissociation constants K_{D1} and K_{D2} in the context of a model where three Co(II) ions bind to the enzyme. This model yielded constants $K_{D1} = 0.10 \pm 0.06$ μM and $K_{D2} = 0.17 \pm 0.04$ μM (Fig. 2*D*). These experiments provide reliable K_D values for the two strongly bound Co(II) eq, being consistent with the weaker binding of a third Co(II), as suggested by the spectroscopic data.

EPR Titration—The perpendicular mode ($\mathbf{B}_{microwave} \perp \mathbf{B}_{static}$) EPR spectra observed upon the addition of Co(II) to apo-BcII (Fig. 3*A*) were found, by difference analysis, to be linear combinations of up to four components. These "basis species" were, in each case, obtained by subtraction of one experimental species from another, as detailed in the legend to Fig. 3*B*, and subsequent computer simulation (Fig. 3*C*) verified that they corresponded to single EPR species and provided spin Hamiltonian parameters. The experimental spectra were reconstructed (Fig. 3*A*) as linear combinations of the basis spectra by using a least-squares fitting routine. Examination of the spin densities of each of the basis species as a function of added Co(II) indicates that two of the basis species became saturated (*i.e.* reached a maximum intensity) during the titration (Fig. S1), and these are assigned to BcII-bound Co(II). The dominant BcII
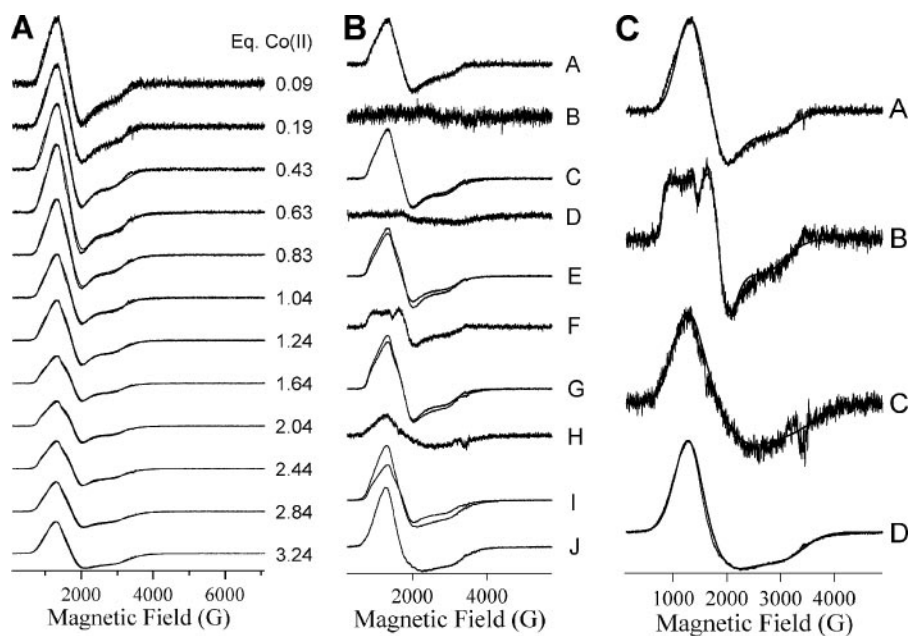
FIGURE 3. **EPR spectroscopic titration of apo-BcII with Co(II).** *A*, experimental EPR spectra of BcII were recorded as a function of added Co(II) and are shown with computer simulations overlaid. Intensities are shown normalized for Co(II) concentration. Simulations were generated by least-squares linear combinations of the theoretical spectra shown as *traces A, B,* and *D* of *panel C,* and the amounts of each species required by the fitting procedure are illustrated in Fig. S1. *B*, difference EPR spectra generated during titration of BcII with Co(II). *Traces A* show overlaid spectra of BcII with 0.43 eq of Co(II), with that of BcII with 0.09 eq of Co(II) multiplied by 4.9. *Trace B* is the difference of the spectra in *A* (*i.e.* 0.43 eq minus 0.09 eq ×4.9). Trace B is shown multiplied by a factor of 3. Analogously, *traces C* are of BcII with 0.83 eq of Co(II) and 0.43 eq of Co(II) (×1.74), and *trace D* is the difference of spectra in *C* (×3). *Traces E* are of BcII with 1.69 eq of Co(II) and 0.83 eq of Co(II) (×0.98), and *trace F* is the difference of the spectra in *E* (×3). *Traces G* are of BcII with 2.44 eq of Co(II) and 1.69 eq of Co(II) (×1.49), and *trace H* is the difference of the spectra in *G* (×3). *Traces I* are of BcII with 3.24 eq of Co(II) and 2.44 eq of Co(II) (×0.82), and *trace J* is the difference of the spectra in *I* (×3). *C*, computer simulations of EPR spectra and difference spectra. *Traces A–D* each show experimental and computer simulated spectra overlaid. The experimental spectra in *A–D* correspond to BcII with 0.19 eq of Co(II) (*A*), *trace F* of B (1.69 eq − 0.83 eq) (*B*), *trace H* of B (2.44 eq − 1.69 eq) (*C*), and *trace J* of Fig. 3B (3.24 eq − 2.44 eq) (*D*). The theoretical spectra *A, C,* and *D* were simulated assuming a spin Hamiltonian $H = \beta g \cdot H \cdot S + S \cdot D \cdot S$, with $S = 3/2$, an axial g_{real}, and $D \gg h\nu$ (a value of 50 cm^{-1} was used, implying that only the $M_S = |\pm 1/2\rangle$ doublet was appreciably populated). A hyperfine term (*S·A·I*) was included in the spin Hamiltonian for the theoretical spectrum of *B*, to account for the $I = 7/2$ ^{59}Co nuclear spin interaction. The resulting EPR parameters were $g_{x,y} = 2.36$, $g_z = 2.44$, $E/D = 0.11$ (*A*); $g_{x,y} = 2.525$, $g_z = 2.65$, $E/D = 0.17$, $A = 8.8 \times 10^{-3}$ cm^{-1} (*B*); $g_{x,y} = 2.22$, $g_z = 2.22$, $E/D = 0.135$ (*C*); and $g_{x,y} = 2.26$, $g_z = 2.28$, $E/D = 0.09$ (*D*).
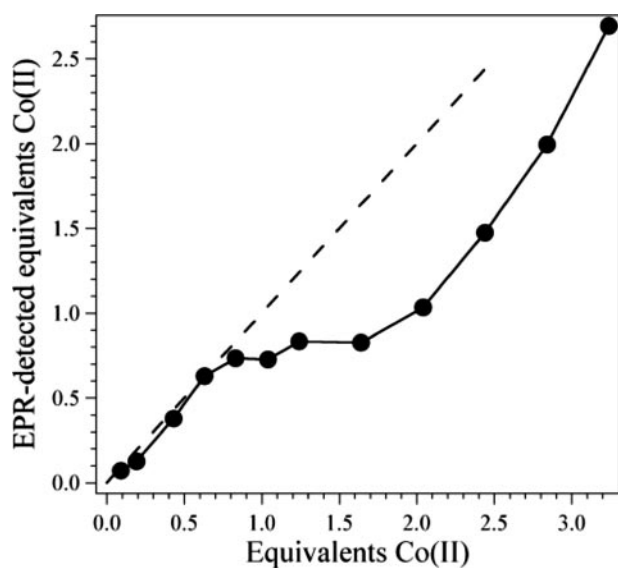

FIGURE 4. **EPR spectrometric titration of apo-BcII with Co(II).** EPR-detected Co(II) (*solid circles*) was quantified by double integration of EPR spectra with respect to Co(II) in 50% 10 mM HEPES buffer, pH 7.5, 50% glycerol. The *dashed line* corresponds to the expected behavior where all added Co(II) is EPR-detectable.

species at low [Co(II)] became saturated upon the addition of 0.8 Co(II) eq, and the EPR signal (Fig. 3C, *trace A*) was simulated, assuming $S = 3/2$, $M_S = |\pm 1/2\rangle$, $D \gg h\nu$ (50 cm^{-1} was used), $E/D = 0.11$, $g_{x,y} = 2.36$, and $g_z = 2.44$; this EPR signal is denoted the "axial" signal due to the low E/D and consequent poor resolution of the $g_{eff.(x,y)}$ resonances. The second species, termed "rhombic" (Fig. 3C, *trace B*), was simulated assuming $S = 3/2$, $M_S = |\pm 1/2\rangle$, $D \gg h\nu$ (50 cm^{-1} was used), $E/D = 0.17$, $g_{x,y} = 2.525$, $g_z = 2.65$, and $A^I = 7/2(^{59}Co) = 8.8 \times 10^{-3}$ cm^{-1}. The intensity of the rhombic signal peaked at around 2 eq of added Co(II) (Fig. S1). A third species, the "broad" species (Fig. 3C, *trace C*; $E/D = 0.14$, $g_{x,y} = 2.22$, $g_z = 2.22$), was isolated by difference; the difference analysis indicated that this species was not observed until the addition of >2 Co(II) eq, but in the least-squares fitting procedure, its inclusion was not statistically justified. The fourth species observed (Fig. 3C, *trace D*; $E/D = 0.09$, $g_{x,y} = 2.26$, $g_z = 2.28$) did not saturate with added Co(II), and, indeed, the signal intensity increased steadily beyond the addition of 2 eq of Co(II). The similarity of this signal to those from Co(II) in buffers and in systems including nonspecifically bound Co(II) suggested that it may not be due to specifically bound Co(II), and we term the signal "free."

A closer examination of the EPR data reveals some interesting phenomena. First, the overall spin density detected by perpendicular mode EPR does not correspond to the amount of Co(II) added (Fig. 4). Up until 0.8 Co(II) eq, the EPR-detected spins increase linearly with added Co(II) and are due to increases in the axial and rhombic signals. Between 0.8 and 1.6 Co(II) eq, however, the overall spin density shows only very little increase in intensity, due to the slow increase in the rhombic signal as Co(II) is added. These data indicated EPR-silent Co(II) and were highly suggestive of the formation of a spin-coupled dinuclear site. Parallel mode ($\mathbf{B}_{microwave} \parallel \mathbf{B}_{static}$) EPR was recorded and derivative-shaped signals were observed with $g_{eff.} \sim 10$ (Fig. 5), consistent with a spin-coupled state ($S' = 0, 1, 2, 3$) of two Co(II) ions. In these signals, the complete line was observable, and, thus, the intensities could be related to the relative amount of this species by simple fitting to a Gaussian line and integration of the Gaussian function. The parallel mode signal appears at around 0.6 eq of Co(II) and increases essentially linearly between 0.6 and 1.6 eq of Co(II) (Fig. S2). Taken together with the observation that the axial and rhombic
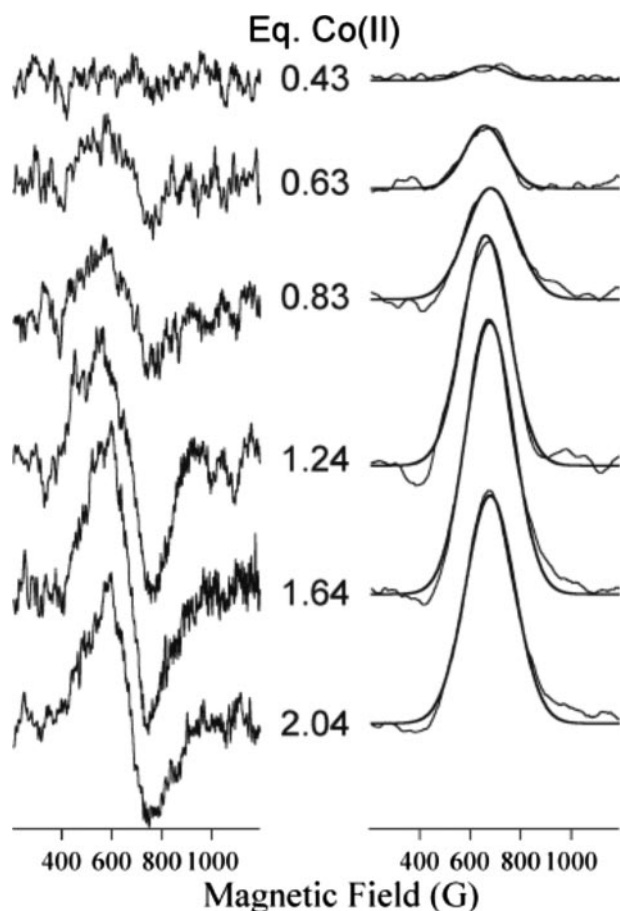
FIGURE 5. **Representative parallel mode EPR spectra of BcII upon addition of Co(II).** The *left panel* shows some experimental first derivative parallel mode EPR spectra of BcII upon titration with Co(II). The *right panel* shows the corresponding absorption spectra, generated by integration of the experimental data. The absorption spectra are shown overlaid with a Gaussian function in each case.

species together account for only 40% of the expected spin density after the addition of 1.6 Co(II) eq (and that the free signal accounts for only another 13%), the parallel mode data provide compelling evidence for a spin-coupled dinuclear species in BcII. This clearly demonstrates that the dinuclear form of the enzyme starts accumulating at Co(II)/enzyme ratios lower than 1.

NMR Titration—The titration of apo-BcII with Co(II) was followed by ^{1}H NMR spectroscopy at 600 MHz at conditions that allow detection of paramagnetically shifted signals (Fig. 6) (33). The spectrum obtained upon the addition of 2 Co(II) eq has been already reported and includes resonances corresponding to metal ligands of the 3H and DCH sites (10). Here we report a spectrum recorded under different conditions (pH 7.5 and low ionic strength) that resembles the one recorded at pH 6.0 and high ionic strength (10). The signal assignments for this spectrum, chemical shifts, and T1 values are summarized in Table 1.

The most downfield-shifted signal envelope centered at 170 ppm is resolved as two separate, broad resonances (A and B) at higher temperatures (Fig. 6A) and can be assigned to the β-CH$_2$ of Cys[221] based on their chemical shifts and line widths (20, 30, 34–39). Resonances D–F are absent when the spectrum is recorded in D$_2$O. An additional resonance corresponding to an exchangeable proton (resonance C) can be detected at lower pH
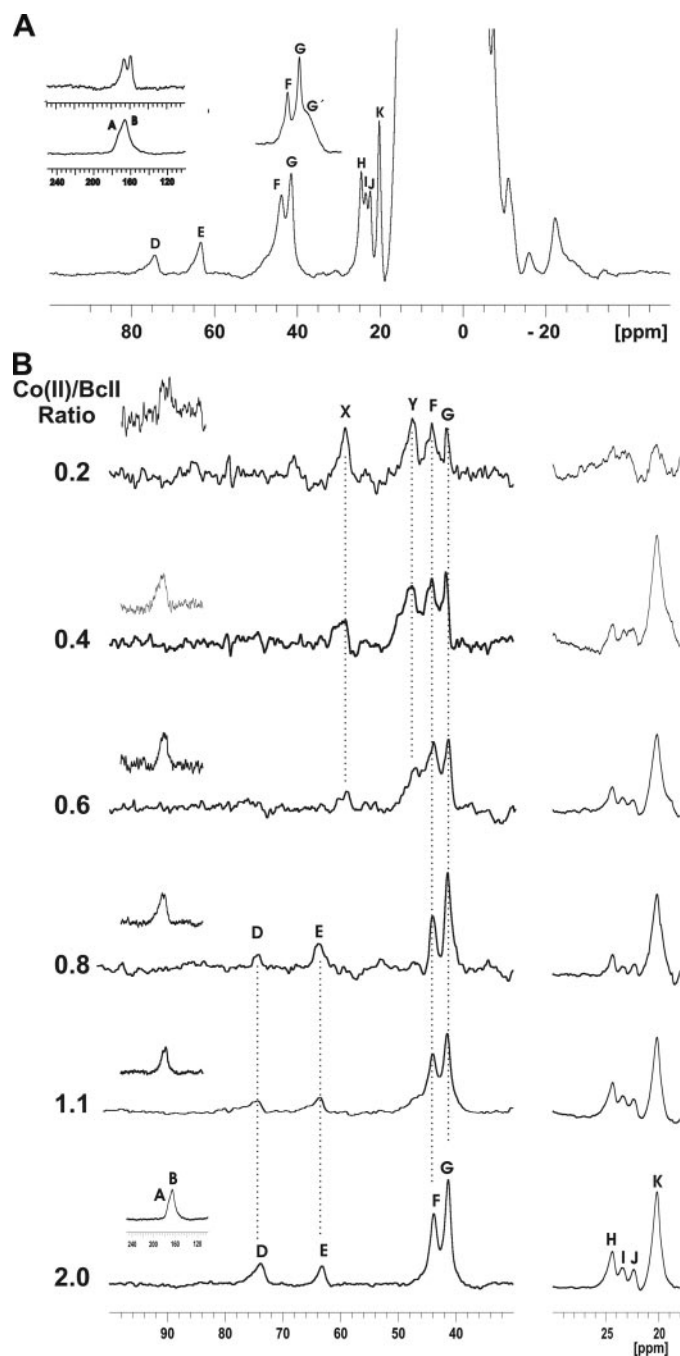

FIGURE 6. **^{1}H NMR spectra of Co(II)-BcII.** *A,* the spectrum was recorded at 600 MHz, pH 7.5, and 301 K in 100 mM HEPES buffer, 0.2 M NaCl. The *inset* at the *left* shows the most downfield region with the β-CH2 Cys resonances recorded at 301 K (*bottom*) and 318 K (*top*). The *inset* at the *right* shows the 50/30 ppm region of the spectrum recorded at 318 K, where signal G' is partially resolved. *B,* ^{1}H NMR titration of apo-BcII with Co(II). ^{1}H NMR spectra recorded at 600 MHz, pH 7.5, and 301 K in 100 mM HEPES buffer, 0.2 M NaCl, at different Co(II)/BcII ratios. The 100/30 ppm and 240/100 ppm spectral regions correspond to spectra recorded using a superWEFT pulse sequence with recycle times of 70 and 10 ms and intermediate recovery delays of 25 and 5 ms, respectively, and were processed with line broadenings of 100 and 600 Hz, respectively. The 30/18 ppm spectral region corresponds to spectra recorded with water presaturation and recycle times of 200 ms and was processed with line broadenings of 50 Hz. Signals X, Y, D, E, and F were not observed when a similar titration was performed in D$_2$O solution.

values, as already reported (10). Signals C–F can be attributed to imidazolic NHs from the His ligands based on their absence in D$_2$O and chemical shifts (20, 30, 34–38). Signal E presents an

TABLE 1

Spectral parameters and assignments of the hyperfine-shifted signals of Co(II)-substituted BcII at 301 K in 100 mM HEPES, pH 7.5, 0.2 M NaCl, unless indicated

Signal	δ	T_1	Assignment
	ppm	*ms*	
A	173	<0.1	Hβ1 (Hβ2) Cys[221]
B	168	<0.1	Hβ2 (Hβ1) Cys[221]
C[a]	73	ND[b]	Hδ1 His[116/196]
D	73.7	7	Hδ1 His[196/116]
E	63.0	7	Hε2 His[118]
F	43.7	7	Hδ1 His[263]
G	41.2	10	DCH site
G′[c]	42	ND	Hδ2 His[118]
H	24.4	20	Hβ1 (Hβ2) Asp[120]
I	23.4	20	DCH site
J	22.4	20	DCH site
K	20.2	30	Hβ2 (Hβ1) Asp[120]

[a] Detected at pH 6.
[b] ND, not determined.
[c] Resolved at 318 K.

NOE with a resonance at 42 ppm, slightly shifted and broader than resonance G. Spectra recorded at higher temperatures allow the detection of a new resonance (G′), partially overlapping with signal G at 301 K (Fig. 6A), that is the one showing the dipolar connectivity with signal E. A reciprocal NOE on signal E was observed when irradiating at 42 ppm. Based on this evidence, we assign resonance G′ to a slowly exchangeable imidazolic CH. Analysis of the crystal structure of BcII reveals that His[118] is bound to the metal ion through its Nδ1, whereas His[116], His[196], and His[263] are coordinated by their Nε2. Thus, resonances E and G′ can be assigned to the Hε2 and Hδ2 from His[118], respectively. Signals C, D, and F therefore correspond to the Hδ1 of the remaining His ligands. Without any further connectivity, we are unable to obtain the sequence-specific assignment of these resonances.

A NOESY experiment revealed that signals H and K are strongly coupled, and K is dipolarly coupled to a resonance at 11 ppm (Fig. S3). The β-CH2 and α-CH of Asp[120] are good candidates for these resonances. The rest of the resonances show no other connectivities and remain unassigned but will be attributed to the 3H or to the DCH site according to the metal site occupancy, as discussed below.

The ¹H NMR spectrum of the species resulting from the addition of 1 Co(II) eq to apo-BcII exhibited the same set of resonances present in the di-Co(II) adduct (Fig. 6B) (*i.e.* corresponding to both sites), in contrast with the situation reported for *B. fragilis* CcrA (20). Based on this, we performed a titration starting at substoichiometric ratios.

Detection of the Cys resonances A and B could be achieved at a Co(II)/BcII ratio as low as 0.2 (Fig. 6B), indicating that the DCH site is being occupied at very low Co(II)/protein ratios, in agreement with the presence of a Cys-Co(II) CT band in the UV-visible titration under these conditions. The set of resonances H–K at 30–20 ppm, some of which correspond to Asp[120], as well as signals F and G, were also present at a 0.2 Co(II)/BcII ratio. Two further resonances (X and Y) at 59.0 and 47.4 ppm that are not present at 2 Co(II) eq, were detected at Co(II)/BcII ratios from 0.2 to 0.6. When a similar titration was performed in D₂O, neither of these resonances was observed, indicating that they correspond to exchangeable protons.

The intensity of all of the resonances observed at 0.2 Co(II)/BcII increases with the further addition of Co(II). A new set of signals is only noticeable beyond 0.6 eq of added Co(II). From this point onward, the exchangeable His resonances D and E can be clearly detected, in line with the disappearance of signals X and Y. For the rest of the titration, the number of detected signals remains the same.

The NMR titration reveals that resonances corresponding to the DCH site (ligands Cys[221] and Asp[120]) grow steadily from 0.2 to 2.0 Co(II) eq, without significant chemical shift perturbations. This is not the case for the signals arising from the 3H site. This suggests that the DCH site is formed in the early steps of the titration with the same structural features present when 2 Co(II) eq are added. Based on this, we feel confident in attributing resonances F and G to the DCH site and therefore assign signal F to the Hδ1 of His[263]. By exclusion, resonance D corresponds to the Hδ1 of His[116] or His[196] (3H site).

Resonances X and Y from 0.2 to 0.6 Co(II) eq can be attributed to imidazolic NHs of the His ligands in a distorted 3H site that rearranges at higher Co(II)/BcII ratios to adopt the final conformation, giving rise to signals D and E. The other two resonances attributed to the 3H site (C and G′) cannot be observed under these conditions. However, the NMR titration shows two clearly distinct behaviors for the 3H and the DCH sites at <0.6 Co(II)/BcII ratios.

It is worth mentioning that the ¹H NMR spectra of Co(II)-BcII at different stoichiometric ratios, temperature, and pH values, for all preparations, showed a low signal-to-noise ratio compared with the one that should be expected for a Co(II)-substituted protein under these experimental conditions. This suggests the existence of a population of Co(II)-BcII with resonances broadened beyond detection that we tentatively attribute to an exchange broadening phenomenon.

DISCUSSION

Metallo-β-lactamases from different subclasses display different metal requirements for function. B2 lactamases are mono-Zn(II) enzymes (40–42), whereas enzymes from subclasses B1 and B3 are fully active in the dimetallic form. Wommer *et al.* have suggested that the mono-Zn(II) form would be the only biologically relevant species for enzymes BcII, BlaB (B1), CphA (B2), and L1 (B3) (6). However, it has been shown that L1 requires two Zn(II) ions to fold properly *in vivo* (43), and other recent kinetic studies indicate that di-Co(II) BcII would be the only active species (19). All of these contrasting findings indicate the need for establishing the metal ion requirements for catalysis. Here we have employed different complementary strategies and techniques to monitor Co(II) binding to apo-BcII to gain insight into the metallated species being formed.

Competition experiments with Mag-fura-2 allowed us to retrieve reliable dissociation constants for 2 Co(II) eq, both being in the submicromolar range. UV-visible spectroscopy reveals that, when the intensities of the bands assigned to these two sites become saturated, a new species accumulates. This species presents a third Co(II) ion bound to a site with submillimolar affinity that perturbs the Co(II) ion at the DCH site, as revealed by a shift in the CT band. Based on these three disso-

ciation constants, the expected populations of the different Co(II)-loaded species can be calculated (Fig. S4). The first and second eq bind with affinities similar to those reported by de Seny *et al.* for Zn(II) and Cd(II) binding using the same approach (8). The proximity of these binding constants indicates that the mono-Co(II) and di-Co(II) species coexist over a wide range of Co(II)/BcII ratios. Instead, de Seny and co-workers informed a dissociation constant of 66.7 μM for the second Co(II) eq, as determined from the UV-visible titration (8). This value resulted from the assumption that the growth of the charge transfer band at 383 nm (Fig. 2*A*) was due to formation of di-Co(II) BcII. Here we have shown that this event takes place after uptake of ~2 Co(II) eq/mol of BcII, thus reflecting the binding of a third Co(II) ion to the enzyme with a dissociation constant around 90 μM.

This complex metal binding scheme is best explored by examining the data collected over distinct regions of added eq of Co(II). The UV-visible titration shows that, upon the addition of Co(II), amounts well below 1 eq of metal ion, features corresponding to both the 3H and the DCH site are present. Di-Co(II) BcII is expected to be formed at <1 Co(II)/enzyme, according to the values of K_{D1} and K_{D2} here reported (Fig. S4). Since the features of the 3H and DCH site in the UV-visible spectra are similar in the mono- and dinuclear species, it is clear that we cannot resort to the spectrophotometric titration to fully address the issue of site occupancy under conditions of limited availability of Co(II).

At Co(II)/BcII ratios of ≤0.6, NMR signals attributable to the 3H and to the DCH site are detected, in agreement with the UV-visible data. The low intensities of the parallel mode EPR signals and the invariance of the positions of the NMR peaks between 0 and 0.6 eq of Co(II) suggest that the majority of Co(II) ions are magnetically and electronically isolated (*i.e.* that BcII is largely in one of two mononuclear states, mono-Co(II)·DCH BcII or mono-Co(II)·3H BcII). The axial signal detected in EPR spectra could account for both sites in the mixture of mono-Co(II) forms. A similar EPR signature has been reported for the di-Co(II) L1 MβL and was interpreted as arising from one or two indistinguishable species (7). This signal also resembles that of Co(II)-ImiS, a lactamase that only bears a DCH site (42).

At Co(II) concentrations over 0.6 eq, a new EPR species appears, the rhombic species, whereas the intensity of the axial signal stays steady. At this point, the dinuclear species starts to accumulate, as indicated by the appearance of a parallel mode signal corresponding to two spin-coupled Co(II) ions. These observations can be reconciled with the UV-visible and NMR titration data if we consider the rhombic species to correspond to one of the metal ions in an uncoupled di-Co(II) species, whereas the other site, mainly unaltered when the uncoupled di-Co(II) enzyme is formed, still gives rise to the axial signal.

The NMR titration reveals that two sites are being initially filled: the DCH site, which retains its structural features along the whole titration, and the 3H site, which experiences a structural change after the addition of 0.6 Co(II) eq, which is then preserved until completion of the metal uptake. This phenomenon takes place at the same Co(II)/BcII ratio at which the coupled di-Co(II) species starts accumulating, as unequivocally

revealed by the EPR titration. This strongly suggests that resonances X and Y correspond to the mono-Co(II)·3H BcII and that D and E are resonances of the 3H site in the di-Co(II) species. The resonances attributed to ligands of the DCH site (A, B, and F–K) are unperturbed along all of the titration. Since EPR reveals no significant di-Co(II) species being formed at very low Co(II)/BcII ratios, this suggests that the DCH site is structurally identical in the mono-Co(II) and di-Co(II) species. It is not surprising that changes in the 3H site are not reflected in different d-d patterns in the visible spectra, since NMR is much more sensitive to structural changes than optical spectroscopy.

Finally, from 2 eq of Co(II) onward, a new EPR signal develops, the broad signal. Simultaneously, the diminution in the intensity of the 343 nm electronic absorption band, with the concomitant growth of a band at 383 nm, indicates that the further addition of Co(II) perturbs the DCH site. These data altogether strongly support binding of a third Co(II) at a weaker site.

In summary, the spectroscopic titrations suggest two *bona fide* metal binding sites in BcII. These two sites together form a dinuclear center with a very small energy difference between an uncoupled state and a very weakly spin-coupled state. Another species with a third Co(II) ion bound, which selectively alters the DCH site, can be formed when excess Co(II) is added. Here we clearly show that at low Co(II)/BcII ratios, there are at least three Co(II)-loaded BcII species (mono-Co(II)·3H, mono-Co(II)·DCH, and di-Co(II) BcII). In the case of the homologous enzyme CcrA from *B. fragilis*, the addition of 1 Co(II) eq gives rise to a single, mono-Co(II) species with the metal ion located in the 3H site (20).

Our picture differs significantly from the one depicted by de Seny *et al.* (8) on Co(II)-BcII based on UV-visible data. The differences are largely attributable to the approach in estimating the K_D values. Our model is strongly supported by EPR data, which allows us to follow the formation of a dinuclear site, and NMR, which provides the identity of the metal ligands at the different metal/BcII ratios explored. Overall, this study implies a new scenario in terms of the metal-loaded species present at different Co(II)/BcII ratios. This prompts for a reevaluation of the proposed catalytic mechanisms for Co(II)-BcII (19, 21, 22, 44, 45).

The present study clearly shows that following reaction kinetics under steady state conditions at different metal/enzyme ratios may be misleading, since the identity of the metal-loaded forms may remain undefined. Thus, non-steady-state kinetic studies and different spectroscopic techniques should be exploited to follow the metal content and localization during MBL turnover. Experiments are under way to address this issue.

The metal content of MBLs *in vivo* is still an unsolved issue (6), particularly when metal ion availability is compromised. Here we have shown that different metallated species can coexist at low metal ion concentrations *in vitro*, and the same situation may hold in the bacterial host. Thus, this scenario should be considered when elucidating the catalytic mechanism or designing potential inhibitors.

REFERENCES

1. Fisher, J. F., Meroueh, S. O., and Mobashery, S. (2005) *Chem. Rev.* **105,** 395–424
2. Crowder, M. W., Spencer, J., and Vila, A. J. (2006) *Acc. Chem. Res.* **39,** 721–728
3. Walsh, T. R., Toleman, M. A., Poirel, L., and Nordmann, P. (2005) *Clin. Microbiol. Rev.* **18,** 306–325
4. Wang, Z., Fast, W., Valentine, A. M., and Benkovic, S. J. (1999) *Curr. Opin. Chem. Biol.* **3,** 614–622
5. Heinz, U., and Adolph, H. W. (2004) *Cell Mol. Life Sci.* **61,** 2827–2839
6. Wommer, S., Rival, S., Heinz, U., Galleni, M., Frere, J. M., Franceschini, N., Amicosante, G., Rasmussen, B., Bauer, R., and Adolph, H. W. (2002) *J. Biol. Chem.* **277,** 24142–24147
7. Garrity, J. D., Bennett, B., and Crowder, M. W. (2005) *Biochemistry* **44,** 1078–1087
8. de Seny, D., Heinz, U., Wommer, S., Kiefer, M., Meyer-Klaucke, W., Galleni, M., Frere, J. M., Bauer, R., and Adolph, H. W. (2001) *J. Biol. Chem.* **276,** 45065–45078
9. Rasia, R. M., and Vila, A. J. (2002) *Biochemistry* **41,** 1853–1860
10. Orellano, E. G., Girardini, J. E., Cricco, J. A., Ceccarelli, E. A., and Vila, A. J. (1998) *Biochemistry* **37,** 10173–10180
11. Dal Peraro, M., Llarrull, L. I., Rothlisberger, U., Vila, A. J., and Carloni, P. (2004) *J. Am. Chem. Soc.* **126,** 12661–12668
12. Park, H., Brothers, E. N., and Merz, K. M., Jr. (2005) *J. Am. Chem. Soc.* **127,** 4232–4241
13. Dal Peraro, M., Vila, A. J., Carloni, P., and Klein, M. L. (2007) *J. Am. Chem. Soc.* **129,** 2808–2812
14. Carfi, A., Pares, S., Duee, E., Galleni, M., Duez, C., Frère, J. M., and Dideberg, O. (1995) *EMBO J.* **14,** 4914–4921
15. Fabiane, S. M., Sohi, M. K., Wan, T., Payne, D. J., Bateson, J. H., Mitchell, T., and Sutton, B. J. (1998) *Biochemistry* **37,** 12404–12411
16. Carfi, A., Duee, E., Galleni, M., Frere, J. M., and Dideberg, O. (1998) *Acta Crystallogr. Sect. D* **54,** 313–323
17. Hemmingsen, L., Damblon, C., Antony, J., Jensen, M., Adolph, H. W., Wommer, S., Roberts, G. C., and Bauer, R. (2001) *J. Am. Chem. Soc.* **123,** 10329–10335
18. Paul-Soto, R., Bauer, R., Frere, J. M., Galleni, M., Meyer-Klaucke, W., Nolting, H., Rossolini, G. M., de Seny, D., Hernandez-Valladares, M., Zeppezauer, M., and Adolph, H. W. (1999) *J. Biol. Chem.* **274,** 13242–13249
19. Badarau, A., and Page, M. I. (2006) *Biochemistry* **45,** 11012–11020
20. Periyannan, G. R., Costello, A. L., Tierney, D. L., Yang, K. W., Bennett, B., and Crowder, M. W. (2006) *Biochemistry* **45,** 1313–1320
21. Bicknell, R., Schaeffer, A., Waley, S. G., and Auld, D. S. (1986) *Biochemistry* **25,** 7208–7215
22. Bicknell, R., and Waley, S. G. (1985) *Biochemistry* **24,** 6876–6887
23. Sambrook, J., Fritsch, E. F., and Maniatis, T. (1989) *Molecular Cloning: A Laboratory Manual*, 2nd Ed., Cold Spring Harbor, NY
24. Hunt, J. B., Neece, S. H., and Ginsburg, A. (1985) *Anal. Biochem.* **146,** 150–157
25. McCall, K. A., and Fierke, C. A. (2000) *Anal. Biochem.* **284,** 307–315
26. Kuzmic, P. (1996) *Anal. Biochem.* **237,** 260–273
27. Bennett, B., Benson, N., McEwan, A. G., and Bray, R. C. (1994) *Eur. J. Biochem.* **225,** 321–331
28. Inubushi, T., and Becker, E. D. (1983) *J. Magn. Reson.* **51,** 128–133
29. Fernandez, C. O., Cricco, J. A., Slutter, C. E., Richards, J. H., Gray, H. B., and Vila, A. J. (2001) *J. Am. Chem. Soc.* **123,** 11678–11685
30. Vila, A. J., and Fernandez, C. O. (1996) *J. Am. Chem. Soc.* **118,** 7291–7298
31. Bertini, I., and Luchinat, C. (1983) *Acc. Chem. Res.* **16,** 272–279
32. Davies, R. B., and Abraham, E. P. (1974) *Biochem. J.* **143,** 129–135
33. Bertini, I., Turano, P., and Vila, A. J. (1993) *Chem. Rev.* **93,** 2833–2932
34. Vila, A. J. (1994) *FEBS Lett.* **355,** 15–18
35. Fernandez, C. O., Niizeki, T., Kohzuma, T., and Vila, A. J. (2003) *J. Biol. Inorg. Chem* **8,** 75–82
36. Crawford, P. A., Yang, K. W., Sharma, N., Bennett, B., and Crowder, M. W. (2005) *Biochemistry* **44,** 5168–5176
37. Donaire, A., Salgado, J., and Moratal, J. M. (1998) *Biochemistry* **37,** 8659–8673
38. Salgado, J., Jimenez, H. R., Donaire, A., and Moratal Mascarell, J. M. (1995) *Eur. J. Biochem.* **231,** 358–369
39. Riley, E. A., Petros, A. K., Smith, K. A., Gibney, B. R., and Tierney, D. L. (2006) *Inorg. Chem.* **45,** 10016–10018
40. Hernández Valladares, M., Felici, A., Weber, G., Adolph, H. W., Zeppezauer, M., Rossolini, G. M., Amicosante, G., Frère, J. M., and Galleni, M. (1997) *Biochemistry* **36,** 11534–11541
41. Crawford, P. A., Sharma, N., Chandrasekar, S., Sigdel, T., Walsh, T. R., Spencer, J., and Crowder, M. W. (2004) *Protein Expression Purif.* **36,** 272–279
42. Sharma, N. P., Hajdin, C., Chandrasekar, S., Bennett, B., Yang, K. W., and Crowder, M. W. (2006) *Biochemistry* **45,** 10729–10738
43. Periyannan, G., Shaw, P. J., Sigdel, T., and Crowder, M. W. (2004) *Protein Sci.* **13,** 2236–2243
44. Badarau, A., Damblon, C., and Page, M. I. (2007) *Biochem. J.* **401,** 197–203
45. Badarau, A., and Page, M. I. (2006) *Biochemistry* **45,** 10654–10666

Evidence for a Dinuclear Active Site in the Metallo-β-lactamase BcII with Substoichiometric Co(II): A NEW MODEL FOR METAL UPTAKE

Leticia I. Llarrull, Mariana F. Tioni, Jason Kowalski, Brian Bennett and Alejandro J. Vila

Access the most updated version of this article at doi: 10.1074/jbc.M704613200

Alerts:
- When this article is cited
- When a correction for this article is posted

Click here to choose from all of JBC's e-mail alerts

Supplemental material:
http://www.jbc.org/content/suppl/2007/08/22/M704613200.DC1

This article cites 44 references, 6 of which can be accessed free at
http://www.jbc.org/content/282/42/30586.full.html#ref-list-1